Characterization of transverse plasma jet and its effects on ramp induced separation

Tang Mengxiao, Wu Yun, Wang Hongyu, Guo Shanguang*, Yang Zhen

Science and Technology on Plasma Dynamic Laboratory, The Air Force Engineering University, Xi'an 710038, People's Republic of China

Email: shanguang_guo@163.com

Submitted to: Experimental thermal and fluid science

Abstract

Plasma synthetic jet actuator (PSJA), which produces pulsed jets, is used to control the shock wave boundary layer interaction at a compression ramp at Ma=2.0. The flow topology of the wall jets from the PSJA is first visualised through particle laser scattering (PLS) photography. The PSJA aperture effect is also examined by comparing the jets out of the apertures of 1,2 mm and 2 mm respectively. The control effect is later investigated by both PLS and particle image velocimetry (PIV).

, which was erupted from different jet apertures of 1.2mm and 2mm, were compared experimentally in a wind tunnel of Mach 2. Further, the interaction between the TPJ and the ramp induced separation was explored. The phase-locked two-component particle image velocimetry (PIV) and particle laser scattering (PLS) were used for flow visualizations. The K-H vortices and hairpin vortices due to the shear stress between the jet plume and high-speed mainstream were identified.The results show that the TPJ in supersonic flow is characterized by two typical parts: the attached jet plume (AJP) and the detached jet plume (DJP). The penetration height of the jet plume, which is closely related to the jet aperture, plays a dominant role in the proportion of the two parts. The higher jet penetration height leads to the more detached jet plume. As for the interaction between the jet plume and separation zone, the attached jet plume was blocked by the separation zone, which formed a recirculation zone and contributed to an expansion of the separation. In contrast, the detached jet plume transited along the shear layer and then enhanced the velocity exchange between the shear layer and mainstream. Ultimately, the reduction of the separation zone was revealed with the overall shear layer reduced. Furthermore, a conceptual model based on two typical morphological features was suggested to reveal the interaction mechanism.

Keywords: transverse plasma jet; supersonic flow; interaction mechanism; shockwave/boundary layer interaction;

1. Introduction

Shock wave/boundary layer interaction (SWBLI) occurs frequently in the supersonic flow. It

may result in flow unsteadiness and large-scale boundary layer separation. These adverse effects reduce aerodynamic efficiency and potentially cause structure failure [1].. Therefore, flow control is needed to address those effects associated with SWBLI. Various passive and active control methods have been proposed so far. The micro vortex generator (MVG), a class of passive control device, is used to eliminate flow separation. Optimization of MVG geometry has been carried out by Zhang[2], Lee[3], and Verma[4]. Lu[5] explored MVG's flow control mechanism . It can be concluded that the counter-rotating streamwise vortices in the wake of MVG play a dominant role in the suppression of shock-induced separation, because a fuller turbulent boundary layer is resulted through the mixing introduced by those vortices. In the category of active flow control[6], the plasma-based actuators gradually gain research attention due to its extraordinary advantages, such as high repetition rate and simple structure. The plasma actuators can be operated various principles including dielectric barrier discharge (DBD), direct current discharge (DCD), laser energy deposition (LED) and pulsed arc discharge (PAD). All the plasma actuators carry out flow control through energy deposition [7]. The plasma actuators have been used for many flow control purposes in the literatures. Yan [8] promoted the supersonic boundary layer transition using the so-called 'thermal bump' (ΔT_w=500K, f=100 kHz) through vortical structures. Falempin and Wang [9-10] investigated the control authority of the steady DCD (2-10 kW and 1-1.5 kW) on shock wave modification. It was found that the resulted thermal choking could weaken the shock wave strength and reduce the shock drag. Webb [11] developed the localized arc filament plasma actuator(LAFPA) and revealed its capability in boundary layer modification. The LED has been shown its potential in suppression of boundary layer separation [12], shock stabilization[13], and wave drag reduction [14].

In the previous work, the plasma synthetic jet actuator (PSJA) has been demonstrated promising capability in SWBLI control[15]. The PSJA features a small chamber with a small orifice on the top. Two electrodes are housed in chamber. The air in the chamber is rapidly heated by arc established in the gap of the two electrodes. Following the sudden pressure and temperature increase, the hot gas leaves the actuator chamber in the form of high-speed jet [16]. The hot jet flow interacts with the boundary layer and further manipulates the shock wave[17]. Zong et al. [18] studied the jet characteristics systematically, and Cybyk et al. [19] has studied its control authority both experimentally and numerically. Later on, Zhang et al. [20] developed the multi-channel discharge technique using the voltage rely circuit as shown in figure 1. This new multi-channel actuators enables increased operation efficiency (200% increase) and allows larger control area. [21]. Narayanaswamy et al. [22] examined PSJA in SWBLI control and found that the characteristic frequency of the shock wave can be forced to be the same as the operating frequency of the PSJA. Yang et al. [23] reported that the PSJA can reduce shock induced separation. Zong et al. [24] recently studied the interaction between the jet produced by the PSJA and a fully developed turbulent boundary layer in the subsonic flow , and visualized the counter-rotating vortex pair (CVP), which energizes the boundary layer. Caruana [25-26] performed a numerical study and demonstrated that the PSJA could reduce the trailing edge separation on a NACA-0015 profile.

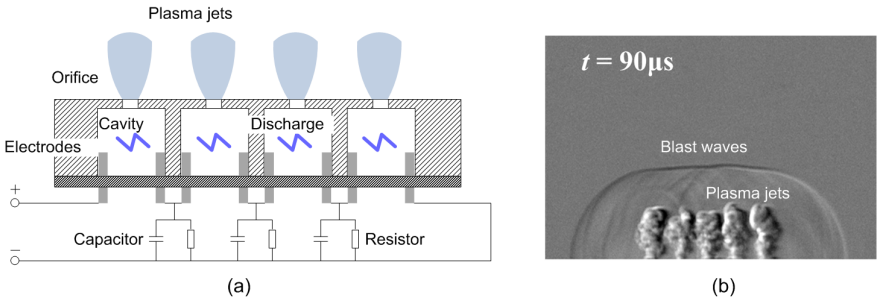

Fig.1 (a) The schematic of actuators with multi-channel discharge circuit; (b) A schlieren snapshot of the plasma jet created by five actuators

Although the PSJA's capability in supersonic flow control has been validated by several studies, an in-depth understanding of its flow control mechanism still has to be strengthenedwhich motivates the present work. The present experimental study is to explore the evolution of the jet flow from the PSJA and its interaction process with the SWBLI established at a 30 degree compression ramp at Ma=2.0. Two different jet apertures (diameter of the oriface), namely 1.2 mm and 3 mm, are used so that the effect of the jet aperture can be revealed.. In the experiment, the particles laser scattering (PLS) photography [do you have a reference for PLS?] is used to visualize the jet evolution in a supersonic freestream and its interaction process.. PIV is further used to study the control process quantitatively.

Note that the PLS method used in this work can be also applied to study the two-phase flows and fluid-particle interaction, such as high heat flux boiling heat transferand bubbling studies[27-30], particle behaviour in the heat exchangers[31-34] and cooling systems and flow behaviour in two-phase systems. For example, the problems about tracking the dispersed nanoparticles in fluids may be well addressed by this method, and so as to description of the status of bubble generation in poor boiling heat transfer.

2. Experimental setup

2.1 Wind tunnel and the models

The experiments were carried out in the FD-20 supersonic wind tunnel at the Air Force Engineering University at Xi'an, China as shown in Fig.2(a). This wind tunnel is a suction type wind tunnel. The flow is driven by the pressure difference between the ambient and the low pressure in the vacuum tank downstream of the test section. The vacuum pressure is set to be 4 kPa in the present experiments. , The total pressure and total temperature are 96.6kPa and 300K, respectively. Multiple layers of screens are installed upstream of the contraction section of the supersonic nozzle so as to reduce the turbulence level. The present contoured convergent-divergent nozzlewith an exit diameter of 300mm generates a supersonic flow of Mach 2.0. The free stream velocity is measured to be

514m/s by PIV under static temperature of 164.4K. The unit Reynolds number is hence estimated to be 1.17×10^7 m^{-1}. Three optical windows are installed for observation. Two of them are on both sides of the test chamber, while the third one is located on the top of the test chamber. The total duration of stable supersonic flow is about 2 seconds under the above settings. A fast response pressure transducer (bandwidth 8 kHz) is used to generate a trigger signal for data acquisition. The flow conditions is summarized in Table 1.

A flat plate model with dimension of 450(L) x120(W) mm^2 is installed at the centre of the test chamber as shown in Fig.2(b). It is used to develop the boundary layer for flow control. According to the experiments in this wind tunnel under similar flow conditions An array of 7 PSJAs are installed along the model span, see Fig. 2(c).The PSJA array is 80mm downstream from the plate leading edge. Each actuator has a Teflon cylindrical cavity and two tungsten electrodes (1 mm diameter). The cavity has a diameter of 6 mm and a height of 4 mm. The electrodes go through the bottom of the cavity and are separated with a gap of 4 mm as depicted in Fig.2(d). . A high-voltage pulsed power and a high-voltage DC power are used to drive the PSJA array [17], They are used to trigger the discharge and charge the capacitor, respectively. As soon as the breakdown voltage is the electrode gap is reached, gas breakdown takes place and the energy stored in the capacitor is deposited through the electric arc, resulting in the Joule heating.. The air in the cavities is then heated rapidlygiving rise to the jet.In order to investigate the effects of jet exit on the performance of PSJA, two jet apertures, namely 1.2 mm and 2 mm,are selected . They are referred to as as C1.2 and C_2 respectively.

According to the previous study in this wind tunnel under similar flow conditions, ratio between the boundary layer thickness and the jet aperture is about δ/d=1.25 [17],

A 30 degree compression ramp is later installed on the flat plate model to establish the SWBLI. It is located 200 mm from the plate leading edge . The angle of 30 degree is chosen so as to generate a large-scale flow separation at ramp corner [17].

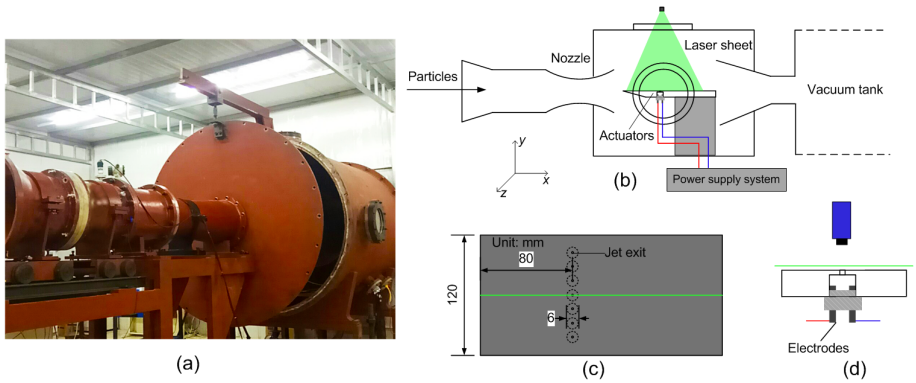

Fig.2 (a) The wind tunnel (b) Schematic of the test facilities (c) The flat plate with actuators: a top view (d) the actuator details; the green regions signify the laser sheet and its location shone on the

top surface of the flat plate

Table1 Flow parameters

Parameters	P_0	T_0	P	T	Ma	ρ	U_∞	Re^{-1}
Value	95.6kPa	296K	12.22kPa	164K	2.0	0.259kg/m^3	514.1m/s	1.19×10^7/m

2.2 The PSJA

The energy deposition in the PSJA is characterized by voltage and current measurements. The voltage is measured by a Tektronics P6015 high-voltage probe and the current is measured by a TCP0030A current probe) s. An oscilloscope with a sampling rate of 100 MHz is used to record the history of voltage and current. In addition, the synchronization between the flow measurement and the discharge is realized by the oscilloscope and the waveform generator, as shown in Fig3. When the wind tunnel starts up, the oscilloscope senses an abrupt pressure rise signal and produces a 5V TTL signal to trigger the waveform generator, which secures synchronization.

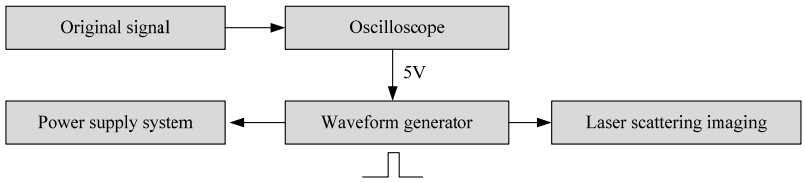

Fig.3 Schematic diagram of the synchronization

2.3 Measurement methods

The phase-locked PLS is used for flow visualisation, while PIV is used to measure the 2D velocity topology.

. Both PLS and PIV make use of the VShot-450 laser and a PCO Imager Pro X camera. The laser beam has energy of 425 mJ/pulse (6 ns pulse width) at a wavelength of 532nm. The laser beam is formed into a sheet of about 1mm thickness. The CCD camera has sensor of 1024x1024 pixels

(check this value) is equipped with a 85 mm focal length Nikon NIKKOR lens.. The camera field of view is adjusted to 90x70 mm^2, resulting in a resolution of 59 μm/pixel. In the PIV measurement, the laser pulses are separation by 0.5 μs.. Cross-correlation and multi-pass iterations are used to calculate the vectors.. The final iteration has an interrogation window of 32×32 pixels with an overlap ratio of 50%..

Different particles are used in LPS and PIV. Water vapor is used as particles in PLS. The effectiveness of water vapor has been validated by Stever[35] and Zhao[36]. The tiny water droplets will condense due to a sudden temperature drop when the flow is expanded through the divergent section of the nozzle [35]. As a result, nanometer-sized particles will be generated in the test section[37]. In the captured PLS images, the jet plume from PSJA is seen as darker region because of sublimation of the water particle at the lower density and higher, whereas the free stream is seeded with the particles.

Droplets of olive oil with a diameter of approximately 1 μm are used as tracer particles in PIV. These particles are generated by the PivPart45-M aerosol generator.. The Stokes number is widely used to evaluate the tracking characteristics of the particles, which is defined as $S_t = \tau_p / \tau_f$. τ_f is the characteristic time of the measured flow and τ_p is the response time of tracer particles. The characteristic time can be calculated as follows:

$$\tau_f = \sigma / U_\infty \tag{1}$$

where σ is the boundary layer and U_∞ is the velocity of the mainstream. The boundary layer in the experiment [17] is 2.5mm and the incoming flow velocity is 514m/s, so the characteristic time τ_f is 4.8μs. And the response time of the 1μm tracer particles can be accurately calculated by the following equation [38]:

$$\tau_p = d_p^2 \frac{\rho_p}{18\mu} \tag{2}$$

where d_p is the diameter of the oil particle, ρ_p is the particle density, and μ is the dynamic viscosity. According to the current working conditions [39], the response time is about 2μs. So the Stokes number is 0.41(<1), which shows a better tracking characteristic.

2.3 Uncertainty analysis

In order to assess the reliability of the measured data, the uncertainty evaluation of the PIV measurement has been studied. Velocity errors are mainly from the image processing of the tracer particles, including the calibration, time interval, flow field and particle image displacement which accounts for the largest proportion[40].Considering the particle image displacement, the uncertainty can be calculated as follows:

$$u_c = c_{\Delta X} \cdot \Delta X \tag{3}$$

where u_c, $c_{\Delta X}$ and ΔX denote the uncertainty, the sensitivity of the particle image displacement and particle image displacement, respectively. The sensitivity value can be defined as the ratio of the camera magnification to the time interval of the laser beam, as shown in equation 4:

$$c_{\Delta X} = \partial u / \partial \Delta X = \alpha / \Delta t \tag{4}$$

where u is the jet velocity, α is the camera magnification and Δt represents the time interval of the laser beam. And the laser pulse, image distortion, sub-pixel fitting and unmatched error of the image can lead to the particle image displacement. The final particle image displacement is estimated as 0.223pix in this experiment. Based on the above formulas, the maximum uncertainty normalized by U_∞ is calculated as 5%.

3 Results and discussion

3.1 Electrical characteristics of the PSJAs

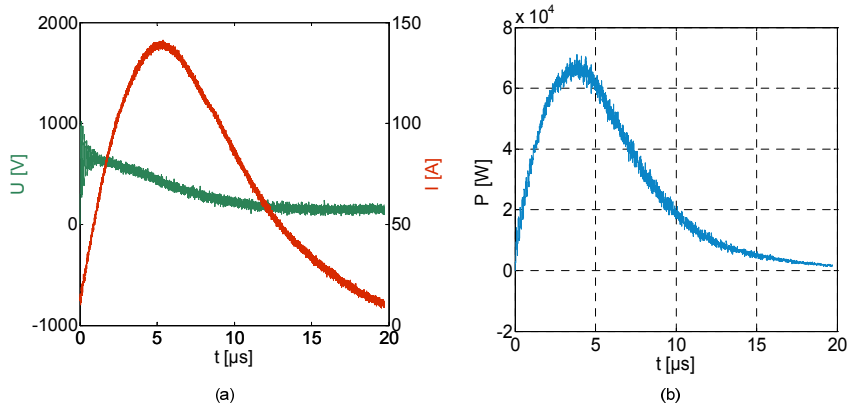

Fig.4 (a) Voltage and current evolutions; (b) power evolution in a pulse of arc discharge using a 2μF capacitor in the circuit, with an 800V voltage supplied to the capacitor.

In order to give an insight into the discharge property of the actuator, the voltage and current are firstly measured over time in experiment. The discharge capacitor has a value C_0 of 2μF, thus the total energy supplied to the actuator could be estimated $E_0 = 0.5 C_0 U^2_{DC} = 0.4$ J [18]. In the baseline study on the jet characteristics, only one actuator is installed so as to minimize the strong electromagnetic interference in the discharge process. The voltage and current evolutions in this case are shown in Fig.4. The characteristics of arc discharge have been reported by Wang[41] in detail. In the present experiment, the discharge duration t_d is about 20μs, which is limited by the capacitance. The energy deposition can be calculated by integration of the instantaneous power over the discharge

duration, as shown in equation 5Thus E_d=???. , Therefore, the discharge efficiency ($\eta_d=E_d / E_0$) is around 0.3 for the current PSJA.

3.2 The jet evolution in supersonic freestream

3.2.1 The PSJA jets through different jet exits

Phase-locked PLS images are acquired to reveal the characteristics of the jet from one PSJA in a Mach 2.0 supersonic flow. In the experiment, delays ranging from 30 μs to 155 μs from the PSJA triggers are selected and the sequence of PLS images showing the evolution of the jet are displayed in Fig.5. Note that these images are recorded in different runs of the wind tunnel. The black blubs over the flow surface suggests the jet body and the subsequent boundary layer structures after the disturbance of the PSJA actuation. The regions are dark because of the sublimation of the ice particles.

At *t*=30 us, the dark blub between x=10~20 mm suggests the jet plume produced by the PSJA. Note that the origin of the streamwise axis is placed at the centroid of the PJSA orifice. The precursor shock wave is also clearly visualized. In the same snapshot, tiny intermittent structures appear close to the wall after the jet plume and grow till the end of the field of view, which is an indication of the boundary layer transition caused by the disturbance from the PSJA actuation. The head of the jet plume moves downstream and reaches x~30 mm at t=50 us, thus the propagation speed of the jet plume is similar as freestream flow speed. Three trailing structures also emerge upstream of the jet plume at the same time. In the following snapshots, the jet plume head maintains its shape despite some deformation. On the other hand, it is rather interesting to see the evolution of the trailing structures. The intermittent blub structure follows closely the head jet plume and grows in size. In the following snapshots till *t*=155 us, a total of 10 structures have emerged. These intermittent trailing blubs are similar as the hairpin vortices in the wake of ramp-shaped vortex generators, which are produced by the Kelvin-Helmoholtz instability. The upstream bulbs are clearly separated by a distance of about 5~7 mm, but the ones near the head blubs are closer and are lifted off the flow surface. This evolution procedure is also quite similar to that of vortices in the MVG wake. As a result, it can be conjectured that, apart from generating the jet plume, the PSJA also generates a localised disturbance acting as a vortex generator. However, further evidence is needed to check this hypothesis observed in the PLS images.

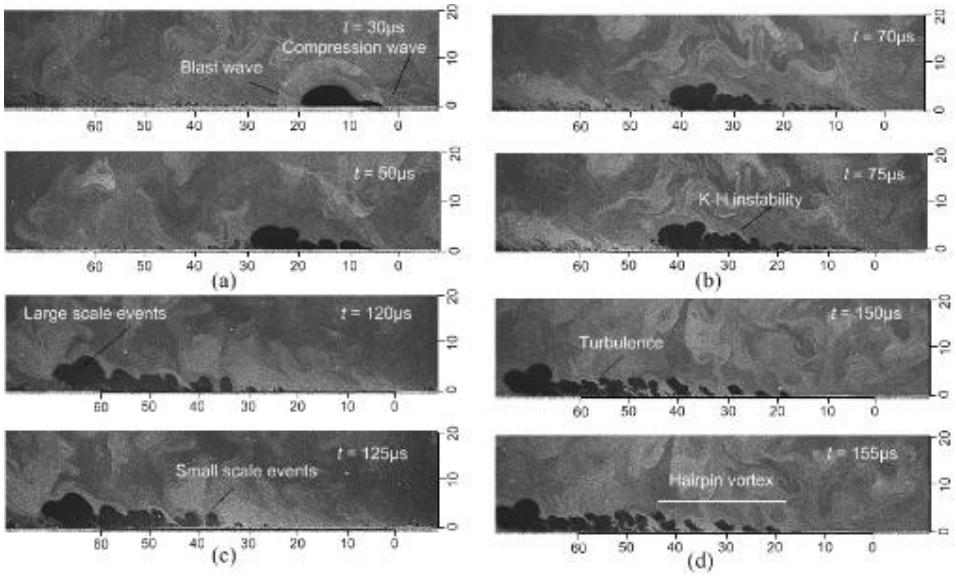

Fig.5 Evolution of jet plume in supersonic flow

The PSJA aperture effect on the jet and the resulted flow is studied by measuring actuators with two orifice diameters, namely d=1.2 mm and 2 mm, which are referred to as D1.2 and D2, respectively. The temporal evolution for the flow structures caused by the two actuators are compared in figure 6. Apparently, D2 with wider jet aperture generates larger jet plume and larger coherent tailing vortices. A larger aperture is beneficial as it allows more heated gas, while a more severe choking condition is resulted by a smaller aperture.

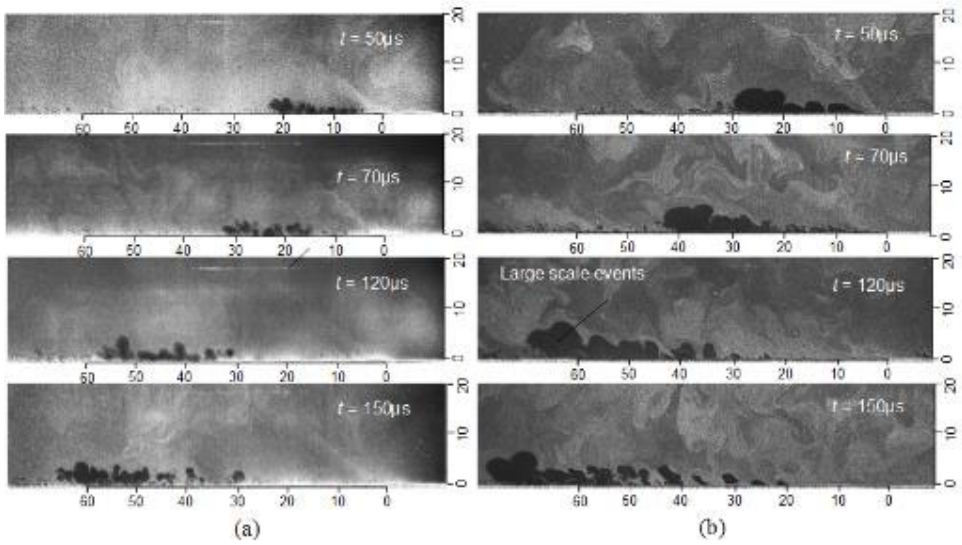

Fig.6 The temporal evolution of the jet plume and the trailing coherent structure after PSJA actuation in one pulse(a)D1.2; (b)D2 (C2 or D2, make sure they are consistent in the paper)

The PLS images of the jet plume and the trailing structures in the following four pulses are further compared in figure 7. These snapshots are of the same phase at a 160us after each pulse trigger. It can be found that similar flow structures are generated in each pulse for both actuators. Comparing the two actuators, D2 obvious generates stronger jet plume, which obtains a height of about 8 mm, while that of D1.2 is only 5 mm. Moreover, the tailing intermittent structures from D2 are also of stronger intensity. These PLS images shown in figure 7 are further averaged for each actuator respectively, see figure 8. The time-averaged structures develop in a wedge pattern. The wedge angle of D2 is about ?? degree while that of D1.2 is ???. This observation reveals that structures from the D2 actuator penetrate more into the free stream. Hence the D2 actuator can be used to improve the control quality.

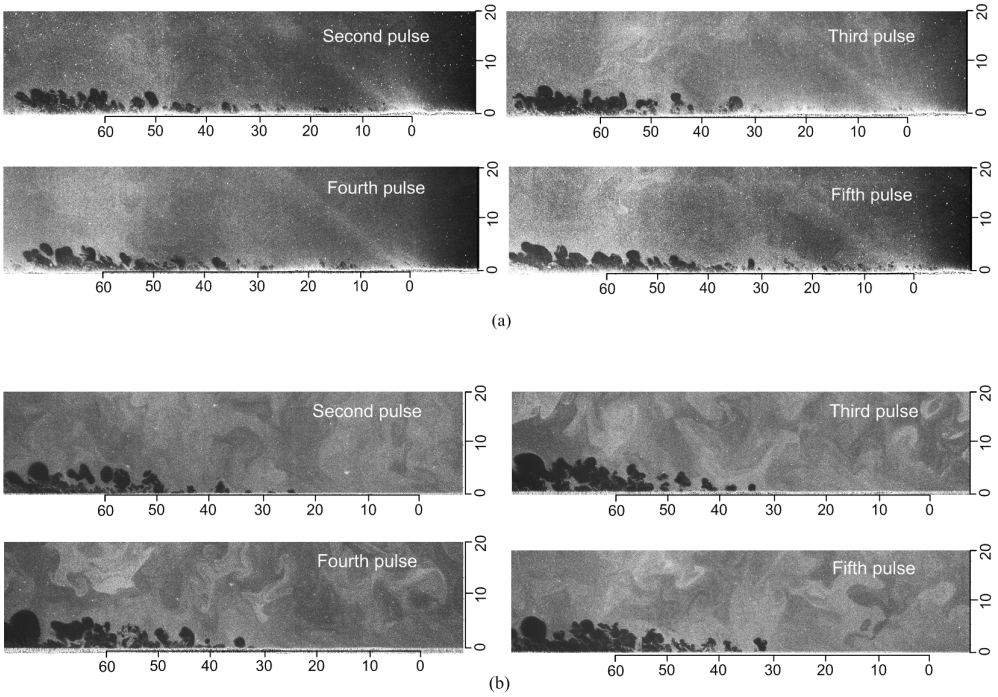

Fig.7 The jet plume and the trailing coherent structures with 160us delay from each pulse trigger in the 2^{nd}~5^{th} pulses.

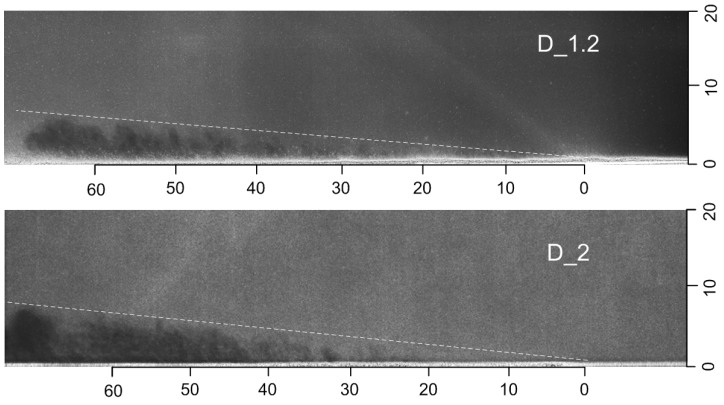

Fig.8 The phase-averaged PLS images for D1.2 and D2.

3.2.2 Interaction between the jet plume and separation zone

In this section, the SWBLI control delivered by the two actuators are examined. A preliminary study on a similar SWBLI control by a transverse plasma jet array has been reported by Wang et al. [7]. The plasma jet is expected to energize the boundary layer and reduce separation. Phase-locked PLS imaging is thus carried out to visualize the control process. The images are recorded with phase delays from 50μs to 500μs as shown in figure 9. Note that the origin is place the foot the ramp. the D The jet plume and its trailing structures can be seen at t=50us for both actuators, they are travelling downstream with the freestream flow to interact with the SWBLI.

********** I start from here **********

Since the resulted structures from D1.2 and D2 travel at speeds similar as the free stream, the jet plumes and part of the trailing vortical structures from both actuators are in the SWBLI region at t=150us. They are induced to move upward as soon as they are past the shock wave. Once the resulted structures fully penetrate the SWBLI zone, the foot of the separation shock wave moves from x=-40 mm to x=-65 mm at t=300 us in the case of D1.2. But, the shock wave has no obvious upstream motion in the case of D2 at the same moment. Moreover, the shaded area around the ramp corner in the D1.2 control is much larger than that controlled by D2. This is perhaps because that the resulted structures from D2 are of stronger intensity and they are attached to the flow surface.

In the next snapshot at t=400 us, the foot portion of the shock waves for both actuators are weakened and not as focused as that before flow control. Meanwhile, the shaded region moves downstream and takes over the ramp surface in both flow fields. The resulted flow structures have passed the SWBLI region and the interaction regions are thinner after the control of both actuators. Finally at t=500us, the SWBLI returns to the uncontrolled status after the flow control plumes and trialing vortices has left the ramp. So far, it can be concluded that both actuators can weaken the shock wave and make the interaction region thinner.

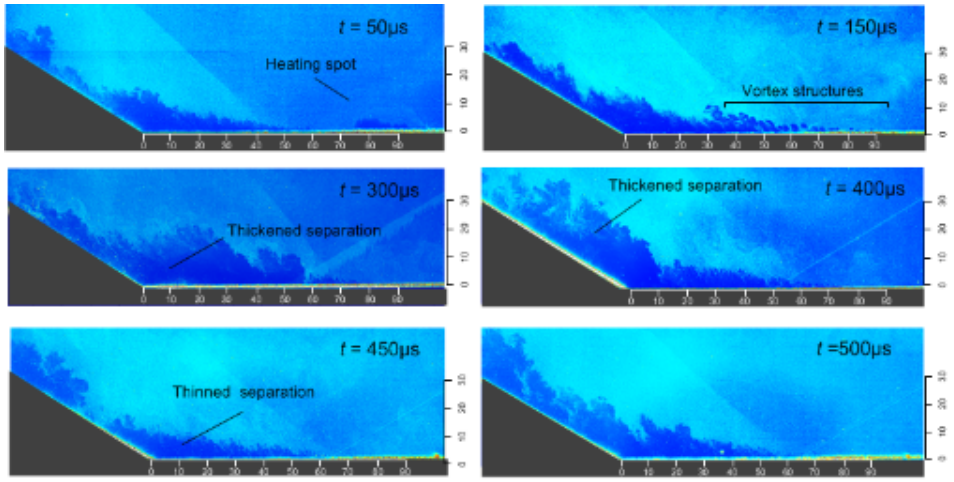

(a)

I don's think it is correct to claim any flow separation here, you can say the corner region 'interaction region'. This technique does not allow you to see the flow revasal, as there is no particle shown in the dark region. Please correct.

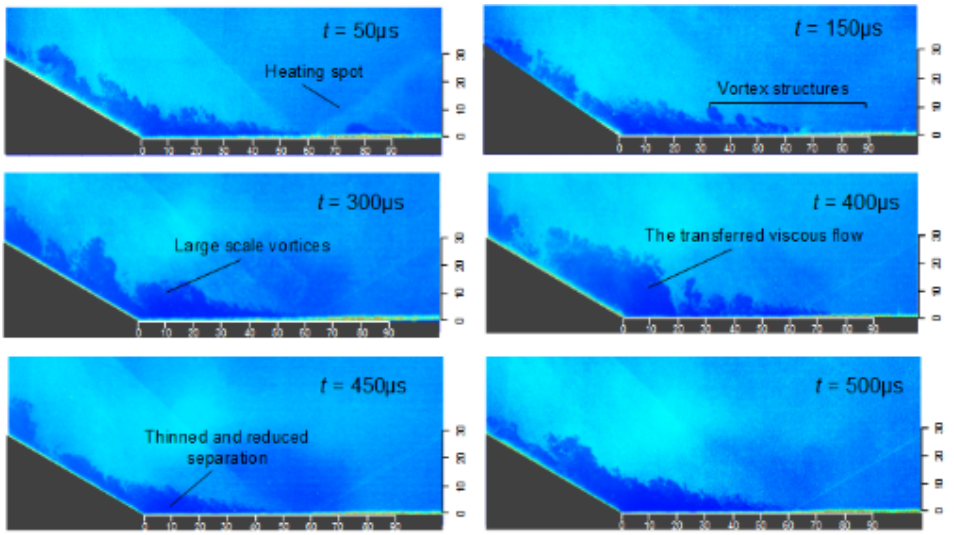

(b)

Fig.9 The temporal evolution of the SWBLI control process: (a) C_1.2; (b) C_2.

The previous instantaneous visualizations

cannot conclude any beneficial effect on the flow separation. Hence, phase averaging is further carried out through 20 snapshot at t=450 us for the two actuators, respectively. The phase-averaged result at t=50 us is also presented and it is used as a reference as the SWBLI is not affected by the plumes and the trailing vortices yet. Comparing the results, it is rather clear that the D2 actuator effectively reduce the length of the interaction region from 55mm to 35 mm, a 36% reduction. Although flow separation alleviation can be concluded, but a potential reduction in separation

reduction can be expected due to a much smaller interaction region. In contrast, the reduction of interaction region is trivial and only a reduction of 5 mm in length. Therefore, the D2 actuator exhibits better control outcome in terms of interaction alleviation.

In order to get better understanding of the interaction between the jet plume and the separated flow, the horizonal plane at 1.5 mm is studied through PLS as shown in figure 11. The instantaneous PLS images reveals the control effect delivered by the D2 actuator. The interaction region at t=0 is shown in Fig.11(a). This snapshot represents the uncontrolled interaction, which has some three-dimensional effect along the model span. The interaction region around the centerline has larger length than that close to the sides. The maximum length appears at around x=+/-10 mm. Moreover, the interaction region is organized by a few stripped zones with extended along the streamwise direction, and the length of the strips are not uniform. . The dominant stripe structures are labelled through the red dotted lines. In the snapshot taken at t=150 us, see Fig11 (b), the traces of the jet plume and the intermittent trailing vortices are clear along the centerline., which were consistent with the streamwise features in *x-y* plane as shown in Fig.5. Beside the central traces of the jet plume and the vortices, there are induced structures of smaller scale, which are not present at t=0.

. The jet plume and trailing vortices move downstream in the following snapshots at t=200 and 350 us. At t=350 us, the interaction region retreat toward the ramp corner with the largest reduction close to the centerline. Meanwhile, the interaction region is still organized as the streamwise strips.

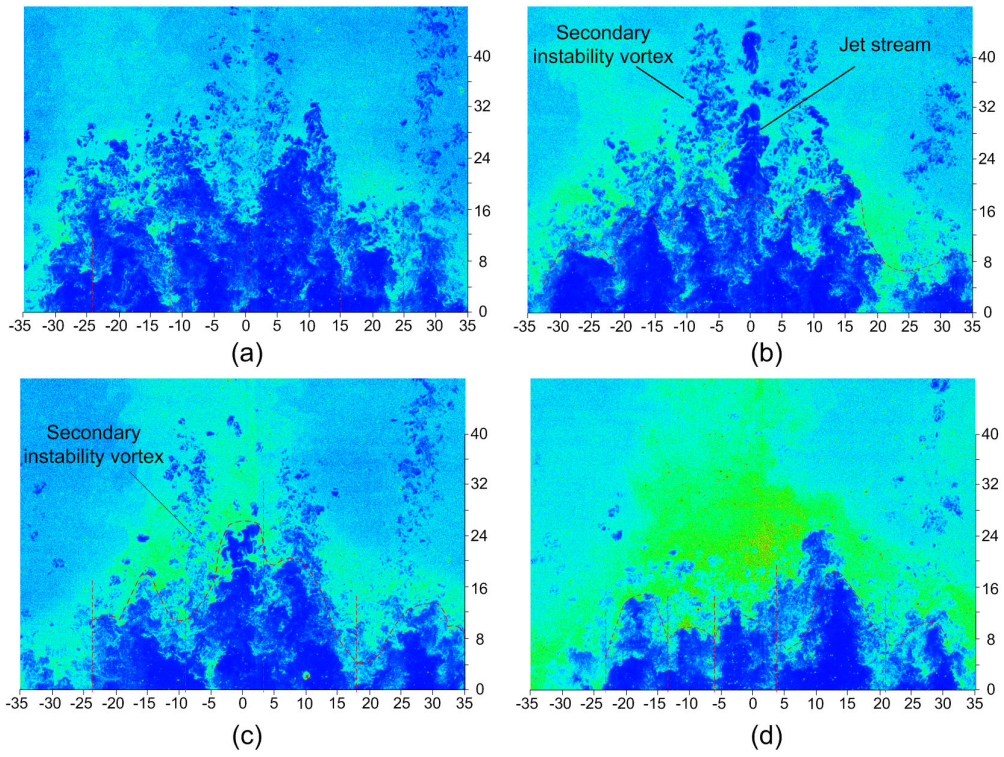

Fig.11 PLS snapshots along spanwise direction at a height of y=1.5 mm: (a) t = 0 (b) t= 150 μs (c) t =200 μs and (d) t =350 μs

3.3The interaction mechanism between the jet plume and the separation zone

3.3.1 The PIV results

The velocity and the vorticity fields of SWBLI control through D_2 actuator are analysed through the phase-locked PIV measurement from t=0 to 300μs. The contours of streamwise velocity at t=0, 150 and 300 us are shown in figure 12(a). At t=0, the shock wave is clearly captured, while the interaction region extends to x=-55 mm, which agrees with the observation through PLS image. The corresponding vorticity contour is shown in figure 12(b) with the zoom-in views provided in figure 12(c). Looking at the vorticity contour at t=0, clear vortex shedding over the ramp is visualised. This is caused by the flow instability at the velocity shear layer between the turbulent region over the ramp and the free stream. The benefit of PIV is that it enables the visualization of the separation. The induced-separation is actually smaller than interaction region and has a length of about 25 mm at t=0. According to the PLS visualization, the plume and trailing vortices are partially in the interaction region. The results is a thicker interaction region and enhanced vortex shedding at t=350us. Eventually at t=450 mm, The interaction region reduced by xx%.

Fig.12 Phase locked velocity and vorticity fields

3.3.2 A conceptual model

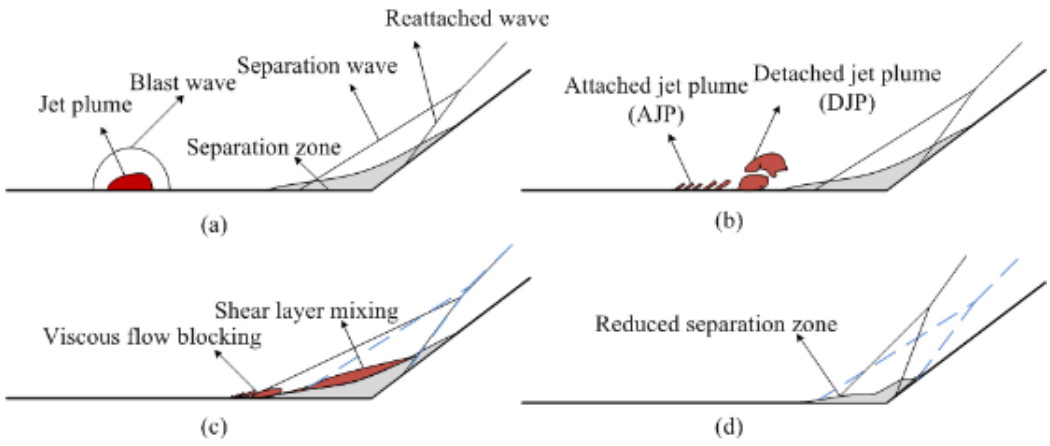

Fig.13 A conceptual model

Based on the analysis above, a conceptual model was drawn in Fig.13. As you can see, the plasma

jet, which consisted of the jet plume and blast wave, was erupted from the cavity first.The jet plume showed its ability to penetrate into the boundary layer. Note that different jet apertures resulted in different penetration height. And in Fig.13(b), the jet plume split into two typical part: the attached jet plume(AJP) which was attached to the wall and the detached jet plume(DJP) which was away from the wall. Results show that the higher jet penetration height leads to the more DJP. Then the AJP was blocked by the separation region, but the DJP transited along the shear layer. Im[44] has put forward the principle that the disturbed boundary layer can suppress the separated flow. We think the DJP can effectively disturb the shear layer. The separation point moved upstream due to the viscous flow blocking, but the DJP enhanced the shear layer mixing, which was good for the velocity exchange. During the process, the separation zone was obviously suppressed.

4 Conclusions

The characteristics of the PSJA and its control effect on SWBLI at a 30 degree compression ramp is examined. The PSJA is found to have an energy deposition of xxx J and an efficiency of ??% through voltage and current measurements. The aerodynamic characteristics is studied by installing the PSJA on a flat plate model. The jet plume is successfully visualized through PLS technique. Moreover, a train of trailing vortices similar as those produced in the wake of vortex generator is also visualised. These trailing vortices are believed to contribute to the control authority. The jet aperture effect is studied by measuring PSJAs with two aperture diameters, namely d=1.2 mm and 2 mm. The PSJA with larger jet aperture is found to generate a stronger jet plume and the trailing vortices. Moreover, the resulted flow structures have deeper penetration. This is understood that a smaller aperture may cause a choking condition in the cavity.

The control effect on SWBLI is finally evaluated through both PLS and PIV. Promising evidence of reduction of the SWBLI region is provided through PLS visualization. However, only the PSJA with 2 mm aperture is effective. The PIV measurement gives some further evidence on the detailed flow structures in the control process. Reduction of the vorticity intensity over the ramp surface is observed.

Acknowledgements

This study is co-supported by the National Natural Science Foundation of China (No. 51522606, 51507187, and 11602302).

Reference

[1]N.T. Clemens, V. Narayanaswamy. Low-Frequency Unsteadiness of Shock Wave/Turbulent Boundary Layer Interactions. Annu.Rev. Fluid Mech. 46(2014) 469-92.

[2] B.B. Zhang, Q.J. Zhao, X.R. Xiang, J.Z.Xu. An improved micro-vortex generator in supersonic flows.Aerospace Science and Technology.47 (2015) 210–215.

[3] S.Lee, E. Loth, H. Babinsky. Normal shock boundary layer control with various vortex generator geometries.Computers & Fluids.49 (2011) 233–246.

[4] S.B.Verma, C.Manisankar. Assessment of Various Low-Profile Mechanical Vortex Generators in Controlling a Shock-Induced Separation.AIAA JOURNAL.55(7)(2017).

[5] F.K. Lu , Q. Li, C.Q. Liu. Microvortex generators in high-speed flow.Progress in Aerospace Sciences. 53 (2012) 30–45.

[6] L.N. Cattafesta, M. Sheplak. Actuators for Active Flow Control.Annu.Rev.Fluid Mech. 43(2011)247–72.

[7] A. Russell, H. Zare-Behtash, K. Kontis. Joule heating flow control methods for high-speed flows.Journal of Electrostatics. 80 (2016) 34-68.

[8] H. Yan, D. Gaitonde, J. S. Shang. Numerical Investigation of Pulsed Thermal Perturbation in Supersonic Boundary Layer.AIAA 2007-3887.

[9] F.Falempin, A.A.Firsov, D.A. Yarantsev, M.A. Goldfeld, K. Timofeev, S.B. Leonov. Plasma control of shock wave configuration in off-design mode of M=2 inlet. Exp Fluids (2015) 56:54.

[10] J. Wang, Y.H. Li, B.Q. Cheng, C.B. Su, H.M. Song and Y. Wu.Effects of plasma aerodynamic actuation on oblique shock wave in a cold supersonic flow. J. Phys. D: Appl. Phys. 42 (8)(2009) 165503 .

[11] N. Webb, C. Clifford, M. Samimy. Control of oblique shock wave/boundary layer interactions using plasma actuators. Exp Fluids. (2013) 54:1545.

[12] Seong-kyunIm, Lydia Wermer. Ramp Separation Response to Laser-Induced Breakdown Disturbed Boundary Layer at Mach 4.5. AIAA 2016-0616.

[13] T. Tamba, H.S. Pham, T. Shoda, A. Iwakawa, and A. Sasoh.Frequency modulation in shock wave-boundary layer interaction by repetitive-pulse laser energy deposition.Physics of Fluids.27(2015)091704.

[14] R. Joarder, U.P. Padhi, A.P. Singh, H.Tummalapalli. International Journal of Heat and Mass Transfer. 105 (2017) 723-740.

[15] H.S. Ko, S.J. Haack, H.B. Land, B. Cybyk, J. Katz, H.J. Kim. Analysis of flow distribution from high-speed flow actuator using particle image velocimetry and digital speckle tomography. Flow Measurement and Instrumentation. 21 (2010) 443-453.

[16]V. Narayanaswamy, L.L. Raja, N.T.Clemens. Characterization of a High-Frequency

Pulsed-Plasma Jet Actuator for Supersonic Flow Control. AIAA JOURNAL 48(2)(2010).

[17]H.Y. Wang, J. Li, D. Jin, M.X.Tang, Y. Wu. Manipulation of ramp-induced shock wave/boundary layer interaction using a transverse plasma jet array. International Journal of Heat and Fluid Flow 67 (2017) 133–137

[18] H.H.Zong, Y. Wu, M.Jia, H.M. Song, H. Liang, Y.H. Li, Z.B. Zhang. Influence of geometrical parameters on performance of plasma synthetic jet actuator. J. Phys. D: Appl. Phys. 49 (2016) 025504 (12pp).

[19] B.Z. Cybyk, J.T. Wilkerson, K.R. Grossman. PERFORMANCE CHARACTERISTICS OF THE SPARKJET FLOW CONTROL ACTUATOR. AIAA 2004-2131

[20] Z.B. Zhang, Y. Wu, M.Jia , H.H. Song, Z.Z. Sun, H.H.Zong, Y.H. Li. The multichannel discharge plasma synthetic jet actuator. Sensors and Actuators A. 253 (2017) 112–117.

[21] Z.B. Zhang, Y. Wu, Z.Z Sun, H.M. Song, M.Jia. H.H.Zong, Y.H. Li. Experimental research on multichannel discharge circuit and multi-electrode plasma synthetic jet actuator.

[22] V.Narayanaswamy, L.L. Raja, N.T. Clemens. Control of unsteadiness of a shock wave/turbulent boundary layer interaction by using a pulsed-plasma-jet actuator.Physics of Fluids.24(2012)076101.

[23] G. Yang, Y.F. Yao, J. Fang ,T. Gan, L.P.Lu. Large-eddy simulation of shock-wave/turbulent boundary layer interaction with and without SparkJet control.Chinese Journal of Aeronautics. 29(3)(2016) 617–629.

[24] H. Zong, M. Kotsonis, Interaction between plasma synthetic jet and subsonic turbulent boundary layer, Phys. Fluids. 29(4) (2017) 045104.

[25] D. Caruana, P. Barricau, P. Hardy, The “Plasma Synthetic Jet” Actuator. Aero-thermodynamic Characterization and first Flow Control Applications.AIAA 2009-1307.

[26] D. Caruana, P. Barricau, C. Gleyzes, Separation control with plasma synthetic jet actuators. Int. J. Aerodynamics. 3(1) 2013 71-83.

[27] M.M. Sarafraz, F. Hormozi.Comparatively experimental study on the boiling thermal performance of metal oxide and multi-walled carbon nanotube nanofluids.Powder Technology. 287(2016)412-430.

[28] M.M. Sarafraz. Experimental investigation on pool boiling heat transfer to formic acid, propanol and 2-butanol pure liquids under the atmospheric pressure.Journal of Applied Fluid Mechanics. 6(1)(2013)73-79

[29] M.M. Sarafraz. Nucleate pool boiling of aqueous solution of citric acid on a smoothed horizontal cylinder. Heat Mass Transfer. 48(2012)611-619.

[30]M.M. Sarafraz, S.A. AlaviFazel. Development of a new correlation for estimating pool boiling

heat transfer coefficient of MEG/DEG/water ternary mixture.Chemical Industry and Chemical Engineering Quarterly. 18(1)(2012)11-18.

[31]M.M. Sarafraz, V. Nikkhah, F. Hormozi.On the convective thermal performance of a CPU cooler working with liquid gallium and CuO/water nanofluid: A comparative study.Applied Thermal Engineering.

[32] M. Kamalgharibi, F. Hormozi, M.M. Sarafraz. Experimental studies on the stability of CuO nanoparticles dispersed in different base fluids: influence of stirring, sonication and surface active agents. Heat Mass Transfer. 52(2016)55-62.

[33]M.M. Sarafraz, V. Nikkhah, F. Hormozi.Low-frequency vibration for fouling mitigation and intensification of thermal performance of a plate heat exchanger working with CuO/water nanofluid.Applied Thermal Engineering. 121(2017)388-399.

[34] M.M. Sarafraz, V. Nikkhah.Fouling formation and thermal performance of aqueous carbon nanotube nanofluid in a heat sink with rectangular parallel microchannel.Applied Thermal Engineering. 123(2017)29-39.

[35] H.G. Stever. Condensation in a high-speed fuild[M].

[36] Y.X. Zhao, S.H. Yi, L.F. Tian. Supersonic flow imaging via nanoparticles. Science in China Series E: Technological Science. 52(12)(2009) 3640-3648.

[37]S. Im, H. Do. The manipulation of an unstarting supersonic flow by plasma actuator. JOURNAL OF PHYSICS D: APPLIED PHYSICS.45(8)(2012) 485202.

[38]X.H. Chen, F. Chen, H. Liu, Tracking Characteristics of PIV Tracer Particles in High Speed Flows. PHYSICS OF GASES. 2(4)(2017)36-45.

[39] D. Ragni, F.F.J. Schrijer, F. Scarano. Particle tracer response across shocks measured by PIV.Exp.Fluids.50(53)(2011).

[40]B.H. Timmins, B.W. Wilson, A method for automatic estimation of instantaneous local uncertainty in particle image velocimetry measurements. Experiments in Fluids. (2012)1013-1031

[41] H.Y.Wang, J.Li, D.Jin, H.Dai, T.Gan, Y.Wu. Effect of a transverse plasma jet on a shock wave induced by a ramp. *Chinese journal of Aeronautics*, 30(6) (2017):1854-1865.

[42]Y.ZHOU, Z.X.XIA, Z.B.LUO. Effect of three-electrode plasma synthetic jet actuator on shock wave control. SCIENCE CHINA Technological Sciences.60(146) (2017).

[43]H.Wei. Transverse jet in supersonic crossflows.Aerospace Science and Technology. 50 (2016) 183–195.

[44] S. Im, L. Wermer. Ramp Separation Response to Laser-Induced Breakdown Disturbed Boundary Layer at Mach 4.5. 54th AIAA Aerospace Science Meeting.